Available online at www.sciencedirect.com
ScienceDirect
International Journal of Thermal Sciences 47 (2008) 1055–1068
International Journal of Thermal Sciences
www.elsevier.com/locate/ijts

A parametric study of phase change material (PCM)-based heat sinks

Xiang-Qi Wang, Christopher Yap, Arun S. Mujumdar *

Department of Mechanical Engineering, National University of Singapore, 10 Kent Ridge Crescent, Singapore, 119260

Received 14 November 2006; received in revised form 30 July 2007; accepted 30 July 2007

Available online 31 August 2007

Abstract

A numerical study is conducted to evaluate the thermal characteristics of a PCM-based heat sink which can be potentially used for cooling of mobile electronic devices such as personal digital assistants (PDAs) and notebooks. The heat sink consists of a conventional, extruded aluminum sink embedded with appropriate PCMs. Some important parameters, such as PCM volume fraction, temperature difference, aspect ratio, and PCM properties, were studied to investigate their effects on the thermal performance of the hybrid cooling system.
© 2007 Elsevier Masson SAS. All rights reserved.

Keywords: Heat sink; Phase change material; Electronic cooling

1. Introduction

Thermal management is recognized as one of the most significant bottlenecks in the development of advanced microprocessors for mobile electronic devices [1], such as personal digital assistants (PDAs), mobile phones, notebooks, digital cameras, etc. Considering the effects of temperature on the reliability of the electronic components, the thermal design must be able to keep the working temperature of such devices below their respective allowable maximum temperatures (generally ranging from 85 to 120 °C) at all times during normal operation. Furthermore, the temperature tolerated by humans [2] has to be considered in the thermal design. Reliability of electronic packages is another challenging factor in the design of mobile electronic devices. Forced convection cooling adds bulk and is not suitable for use in mobile devices. One alternative passive means of electronic cooling is the use of phase change materials (PCMs), which are light and have a high latent heat of fusion.

There are several benefits to using PCM-based cooling devices. First, PCMs can be used for cooling single as well as discrete heat loads. Second, they provide a completely passive method or a partially active method (when connected to convective heat sink). Third, the temperature range of operation can be easily designed for a specific electronic component by choosing suitable PCMs. Last but not least, considering their high latent heat of fusion, they can be used as backup for some periods during extreme thermal environments, e.g., when the primary thermal management system is inactive. Gong and Mujumdar [3–9] have carried out a series of numerical studies on heat transfer during melting and freezing of single and multiple PCMs. Casano and Piva [10] investigated the periodic phase change process of a plane PCM slab numerically and experimentally. They claimed that comparison between numerical and experimental data showed good agreement. However, the numerical method used is just one-dimensional code that neglected the effect of free convection. Jiji and Gaye [11] also analytically examined one-dimensional solidification and melting of a slab with uniform volumetric energy generation. However, the low thermal conductivity of PCMs presents a significant challenge in the design of PCM-based electronic cooling systems.

In order to overcome this inherent drawback of PCMs, various heat transfer enhancement techniques have been proposed. These methods include use of partitions/fins, graphite/metal matrices, dispersed high-conductivity particles in the PCM, and micro-encapsulation of PCM, as discussed by Velraj et al. [12] and Zalba et al. [13]. Use of PCM-based heat sinks is an effective and practical way for cooling applications for electronic devices, as discussed by Pal and Joshi [14]. The concept is simple as it uses specific cavities filled with PCMs as the heat sink. The fins of the heat sink can be used as partitions within the PCM volume to improve their thermal performance, while the

* Corresponding author. Tel.: +65 6516 4623; fax: +65 6779 1459.
E-mail address: mpeasm@nus.edu.sg (A.S. Mujumdar).

1290-0729/$ – see front matter © 2007 Elsevier Masson SAS. All rights reserved.
doi:10.1016/j.ijthermalsci.2007.07.016

PCMs keep the temperature of the electronic device below a critical temperature—usually the junction temperature of silicon, which is 90 °C [15,16]. PCM-based heat sinks can effectively store the dissipated heat from the components via phase change from solid to liquid. Molten PCM can be re-solidified by dissipating heat to the surroundings when the electronic devices are idle [17]. To achieve effective cooling it is important to ensure that the operation period of the electronic devices does not exceed the time of full melting.

O'Connor and Weber [18] measured the thermal performance of a PCM heat sink. Pal and Joshi [14] studied computationally and experimentally melting of a PCM, *n*-triacontane ($C_{30}H_{62}$), in a side uniformly heated (isothermal wall) tall enclosure of aspect ratio 10 for avionics applications. Leland and Recktenwald [19] numerically optimized the geometry of a PCM heat sink used for extreme environment with neglected effect of convection in the molten PCM, edge effects on the ambient boundary, and heat spreading effects in the heat sink base. Zheng and Wirtz [20–22] used numerical models and experiments to optimize the performance of phase change heat sinks. The PCM they used is the polyalcohols pentaglycerine [PG] ($C_5H_{12}O_3$) with melting point of 83 °C. According to Lamberg and Siren [23], there are three stages in the melting process: pure conduction from the end-wall and the fins, conduction from the fin with some natural convection from the end-wall, and finally only natural convection from the fin.

Tan and Tso [24] experimentally studied the cooling of mobile electronic devices using a heat storage unit filled with *n*-eicosane inside the device. They observed that the effectiveness of the heat storage unit depends on the amount of PCM used. The larger the amount of PCM, the longer it can stabilize the temperature of the mobile electronic device, as expected. They also found that different orientations of the heat storage unit significantly affect the temperature distribution. Krishnan et al. [25] proposed a hybrid heat sink which combined an active plate fin heat sink with the tip immersed in a passive PCM. The one dimensional fin equation was used for analysis. Akhilesh et al. [26] presented a thermal design procedure (using a scaling analysis of the governing two dimensional unsteady energy equations) to maximize the energy storage and operating time for a composite heat sink consisting of an elemental heat sink, PCM, and highly conductive base material. Shatikian et al. [27] numerically investigated melting of PCM in a heat sink and generalized the results through dimensional analysis.

The modeling of phase-change processes presents a significant challenge due to complexity and conjunction of the involved physical phenomena. Some important factors, which are generally neglected by previous studies, should be involved during the numerical analysis, e.g. volumetric expansion due to the phase change, convection in the liquid phase, and motion of the solid in the melt due to density differences. Considering the computing-intensive nature of these numerical simulation, it is not uncommon to use a two dimensional model for three-dimensional situations if the three dimensionality is confined to a small region of the total domain. Huang et al. [28] compared 2D and 3D heat transfer models of PCM and found that the 2D model can reflect accurately the predictions made using the 3D model for simple line-axis systems.

This study is an attempt to overcome some of the above-mentioned limitations, and to solve the complete conservation equations simultaneously for solid fins, solid and liquid PCM, and air, while allowing for PCM expansion, convection in the fluid media, and solid phase motion in the liquid. This method has been implemented successfully by Shatikian et al. [27]. In the present work, similar approach is used for a detailed parametric investigation of the conjugate heat transfer problem of melting and solidification in a small PCM-based heat sink cooling system. Following comparison between heat sink without PCMs and that with PCMs, a series of parametric studies are carried out for the purpose of optimized design of such hybrid systems.

2. Model and analysis

A schematic diagram of the two-dimensional physical model is shown in Fig. 1. The heat sink is made of aluminum and the

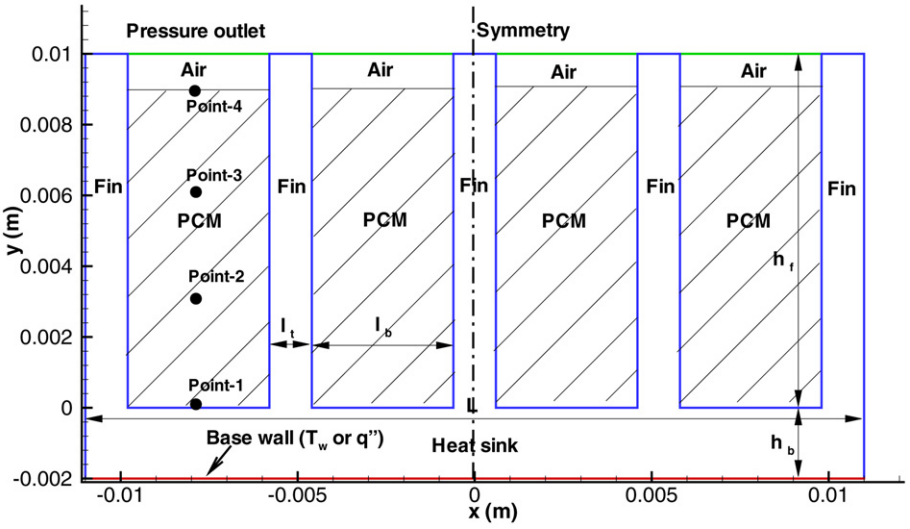

Fig. 1. Physical model.

cavities inside hold and store the solid PCM. The heat sink unit is 22 mm wide (L) and 12 mm high (H) with 2 mm thick (h_b) bottom base with uniform temperature, T_w. Five aluminum fins of 1 mm thickness (l_t) mounted over the heat sink to form four cavities with equal width, l_b (4 mm). The PCMs are filled in the aluminum case with a specific depth (h_t) of the 10 mm cavities in heat sink. The top of the aluminum cavities are open to ambient to allow expansion of PCM volume during melting. Thus, it is assumed that heat is transferred between the PCM and the base, the fins, the end walls and the ambient air. Heat transfer from the fin tips to the ambient is not considered. Following the analysis of Shatikian et al. [27], a relatively small volume PCM-based heat sink system is chosen since such heat sinks are currently used in cooling application of electronic components. A hybrid system with addition of PCM in the heat sink is expected to improve the thermal performance of the sink.

In order to overcome the above-mentioned limitations such as neglect of natural convection in liquid PCM, and neglect of the effect of ambient air on the melting of PCM, a numerical approach is proposed to model the processes that occur inside the fins and the end walls, the PCM, and surrounding air simultaneously, and also the influence of diffusion in the liquid PCM volume. Heat conduction solution is obtained for the fins and the end walls, while convection equations are solved for air/liquid PCM two-phase media under laminar flow assumption. For the melting and solidification of PCM, the well-known enthalpy-porosity approach [29,30] is employed, wherein the porosity in each cell is set equal to the liquid fraction in that cell.

For the aluminum fins, only 2D conduction is considered. Accordingly, the energy equation is:

$$\frac{\partial}{\partial t}(\rho_s h) = \frac{\partial}{\partial x_i}\left(k_s \frac{\partial T}{\partial x_i}\right) \tag{1}$$

For the PCM-air system with a moving internal interface but without inter-penetration of the two fluids, the volume-of-fluid (or VOF) model is used [31]. In this model, if the nth ($n = 1$ for liquid PCM phase, $n = 2$ for air phase) liquid's volume fraction in the computational cell is denoted as α_n, then the following three conditions are possible: if $\alpha_n = 0$ the cell is empty of the nth liquid; if $\alpha_n = 1$ the cell is full of the nth liquid; and if $0 < \alpha_n < 1$ the cell contains the interface between nth fluid and one or more other the two liquids. Accordingly, the governing equations used for modeling the PCM-air hybrid system are:

$$\text{continuity:}\quad \frac{\partial \alpha_n}{\partial t} + u_i \frac{\partial \alpha_n}{\partial x_i} = 0 \tag{2}$$

$$\text{momentum:}\quad \frac{\partial}{\partial t}(\rho_n u_i) + \frac{\partial}{\partial x_j}(\rho_n u_j u_i) = -\frac{\partial p}{\partial x_i} + \frac{\partial}{\partial x_j}\left[\mu\left(\frac{\partial u_i}{\partial x_j} + \frac{\partial u_j}{\partial x_j} - \frac{2}{3}\delta_{ij}\frac{\partial u_l}{\partial x_l}\right)\right] + \rho_n g_i + S_{n,i} \tag{3}$$

$$\text{energy:}\quad \frac{\partial}{\partial t}(\rho_n h) + \frac{\partial}{\partial x_i}(\rho_n u_i h) = \frac{\partial}{\partial x_i}\left(k_n \frac{\partial T}{\partial x_i}\right) \tag{4}$$

where α_n is the nth fluid's volume fraction in the computational cell, ρ_n, k_n, and μ_n are the density, thermal conductivity, and dynamic viscosity of the nth fluid, respectively. $S_{n,i}$ is the momentum source term, which is equal to zero for air phase, but $S_i = -A(\phi)u_i$ for PCM phase. Here $A(\phi)$ is the "porosity function" defined by Brent et al. [30] to make the momentum equation mimic Carman–Kozeny equations for the flow in porous media: $A(\phi) = C(1-\phi^2)/(\phi^3+\varepsilon)$ with $\varepsilon = 0.001$ and $C = 10^5$ used here. Also, u_i is the velocity component, x_i is a Cartesian coordinate, and h is the specific enthalpy defined as, $h = h_{\text{ref}} + \int_{T_{\text{ref}}}^{T} c_p \, \mathrm{d}T$, and the enthalpy change due to the phase change $\phi\Delta H$, at reference temperature T_{ref}, c_p is the specific heat, ΔH is the latent heat of melting of the PCM, and ϕ is the liquid fraction during the phase change which occurs over a range of temperatures $T_{\text{solidus}} < T < T_{\text{liquidus}}$.

Since the proposed PCM-based heat sink problem is time-dependent, initial and boundary conditions must be set appropriately before the calculation starts. With reference to the origin indicated in Fig. 1,

$$\begin{aligned}
&\text{I.C.: } t \leqslant 0, \quad T = T_{\text{int}}, \text{ for } -\frac{L}{2} \leqslant x \leqslant \frac{L}{2};\\
&\qquad\qquad -h_b \leqslant y \leqslant h_f\\
&\text{B.C.: } t > 0, \quad T(y = -h_b) = T_w \text{ or } \left(k_s \frac{\partial T}{\partial x}\right)_w = q''_w\\
&\qquad\qquad h'\left(x = \pm\frac{L}{2}\right) = h'_a\\
&\qquad\qquad \text{Air top: } P_{a,\text{out}}(y = h_f) = P_{\text{amb}}\\
&\qquad\qquad \text{Fin top: } h'(y = h_f) = h'_a
\end{aligned}$$

Note that T_w is higher than the melting point of the PCM inside the heat sink ($T_w > T_m$) as well as the initial temperature ($T_w > T_i$), so heat can be transferred from the bottom surface to the top fins and PCMs and results in melting of PCMs. And vice versa for freezing process. For pure melting cases, the fins were set as insulated boundary ($q'' = 0$); while for cyclic melting/solidification cases, the fins were put in an assumed heat transfer coefficient (h'_a).

As shown in Table 1, for air, the density depends on its temperature. For aluminum solid phase, constant properties are selected. For PCM phase (PCM is paraffin wax here), considering the computational continuity during phase change, the density can be expressed as

$$\rho_{\text{PCM}} = \frac{\rho_L}{\beta(T - T_m) + 1} \tag{5}$$

where ρ_L is the density of PCM at the melting temperature T_m, and β is the thermal expansion coefficient ($\beta = 0.001$ can be used as Humphries and Griggs [32]). Also, as shown in Table 1, the thermal conductivities of liquid and solid PCM are $k_f = 0.21$ W/m-K and $k_s = 0.12$ W/m-K, respectively. The melting point T_m and latent heat ΔH are also listed in the table.

The dynamic viscosity of the liquid PCM (paraffin wax) is given by

$$\mu = 0.001 \times \exp(A + B/T) \tag{6}$$

where $A = -4.25$ and $B = 1790$ following Reid et al. [33]. Hence, the viscosity of liquid PCM is $\mu = 0.001 \times \exp(-4.25 + 1790/T)$ kg/m-s.

The numerical simulation has been carried out using Fluent 6.2 software [34]. The PISO algorithm was used for

Table 1
Properties of paraffin wax, aluminum, and air

	ρ (kg/m^3)	c_p (J/kg-K)	k (W/m-K)	T_m (°C)	ΔH (J/kg)
Paraffin wax	$\frac{750}{0.001(T-319)+1}$	2890	0.21/0.12	46–48	173 400
Aluminum	2719	871	202.4	–	–
Air	$1.2\times10^{-5}T^2 - 0.01134T + 3.498$	1006.4	0.0242	–	–

Table 2
Thermophysical properties of n-octadecane and polycarbonate [36,37]

Properties	ρ (kg/m^3)	k (W/m-K)	C_p (J/kg-K)	μ (Pa-s)	L (J/kg)	T_m (°C)
n-octadecane (l)	746	0.157	2200	3.878×10^{-3}	241 360	28.0
n-octadecane (s)	814	0.390	1900	–	–	27.0
polycarbonate	1200	0.20	1200	–	–	–

pressure–velocity coupling. Four sets of grids (40 × 40, 80 × 80, 160 × 160, and 320 × 320) were used for the grid independence test and the evolution of melt fraction with time was monitored for comparison. The compared results shows that the set 160 × 160 is suitable since the calculated difference between it with the case of 80 × 80 is less than 1%. Furthermore, similar careful examination was conducted for the time step size ($\Delta t = 1$, 0.1, 0.05, 0.01 s). To limit the numerical error of monitored melt fraction in range of 1%, $\Delta t = 0.01$ s was selected for our simulation. The convergence was also checked at each time step, with the convergence criterion of 10^{-4} for velocity components and 10^{-7} for energy.

3. Results and discussion

The numerical method has been validated for the experimental setup proposed by Pinelli et al. [35]. The test section consisted of a hollow vertical cylinder of polycarbonate (outer diameter of 150 mm, inner diameter of 140 mm, and height of 210 mm). Only 51.1 mm of the bottom part of the cylinder was used for initial storage of PCM (99% pure n-octadecane, or n-$C_{18}H_{38}$). Since a true constant temperature boundary condition could not be achieved in the experiment, they measured the top and bottom boundary temperatures as well. Similar to their numerical solution [10,35], the top and bottom measured temperature values were imposed as boundary conditions. The thermal coupling between the cylinder and the ambient was included through an overall heat transfer coefficient of 0.5 W/m^2-K. Our numerical model also included the above-mentioned PCM-air system to consider the effect of the top air and the expansion of PCM itself. The properties of n-octadecane and polycarbonate [36,37] are listed in Table 2. The properties of air are listed in Table 1. Note that the variation of property values in liquid and solid phase of PCM was imposed using piecewise linear interpolation to avoid numerical discontinuity.

A two-dimensional axisymmetric model was employed. Eight monitored points at the centerline ($y = 0$, TC1: $x =$ 0 mm, TC2: 8.4 mm, TC3: 21.5 mm, TC4: 36.4 mm, TC5: 50.8 mm, TC6: 59.1 mm) were used to capture the local temperature evolution with time. As compared to the numerical

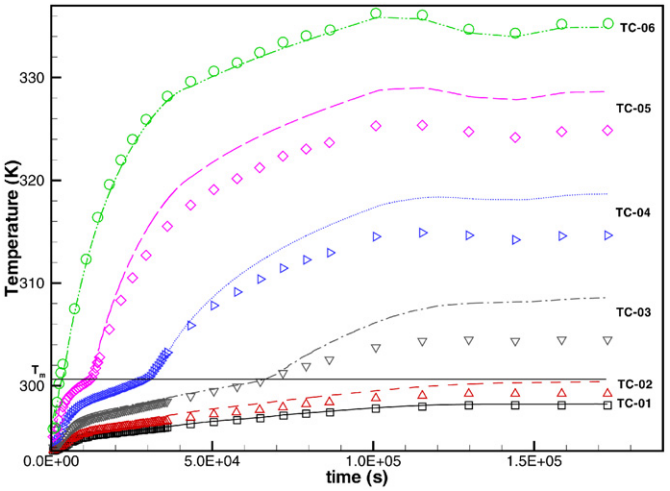

Fig. 2. Comparison of experimental [35] and numerical temperature distributions.

results from Pinelli et al. [35], the agreement in the current study is much better. However, the discrepancy is still obvious, especially at large time. The possible reasons can be attributed to 2D simplicity, deviation in interpolation of boundary temperature values, lack of reliable information about the properties, and numerical errors caused by long calculation periods.

Another test case investigated was the three-dimensional model. The experimental setup proposed by Zivkovic [38] was used for purpose of comparison. As discussed in [38], the setup consisted of a rectangular container (length of 100 mm, width of 100 mm, and thickness of 20 mm) with filled calcium chloride hexahydrate. It was well insulated on the lateral sides using polystyrene. A thermocouple was put in the center of the container to monitor the temperature variation. A three-dimensional numerical model was employed to reproduce the experimental conditions within constant temperature bath. The initial temperature, T_i, was 17.9 °C, while the bath temperature was set to $T_\infty = 60$ °C. The convective heat transfer coefficient between the bath and the container wall was calculated to be $h' = 16$ W/m^2-K [38].

Fig. 3 shows the comparison of local temperature at the center of the container between the numerical results and the

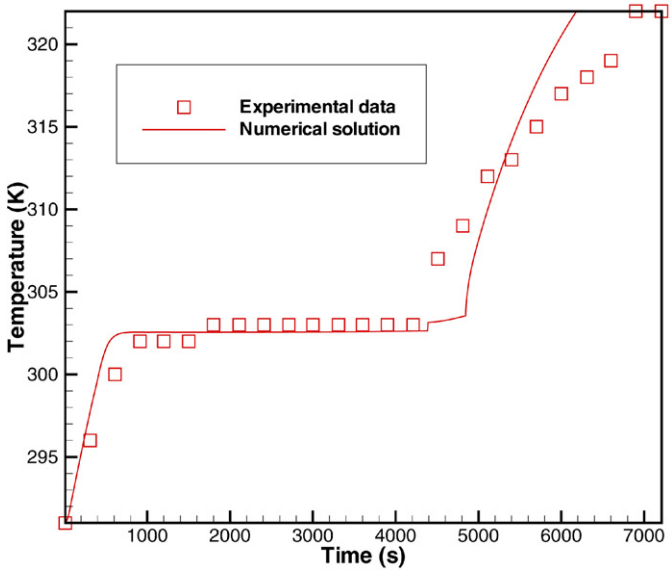

Fig. 3. Evolution of the temperature at the center of the rectangular container: comparison of experimental data [41] and 3D numerical results.

experimental data from Zukowski [38]. The agreement is well within uncertainties as indicated in [38], although the melting rate from the simulation is slightly higher than that from experiment. The discrepancy is caused by the neglect of wall conduction in their mathematical model.

The velocity contours at different slices at $t = 100$ min are displayed in Fig. 4. It is clearly indicated that the natural convection within the melt is important and cannot be ignored. Furthermore, it can be concluded that the velocity contours at different slices are nearly same except close to the wall, where velocity values are relatively small due to effect of the wall. That means a 2D model should capture the phenomena well since the variation in the additional dimension is negligible, while considerable computation time saved. Consequently, in the following sections, only the 2D model was used.

In the following section, a series of parameters was chosen for detailed investigation, the results of the parametric study are discussed and analyzed. Note that paraffin wax (Table 5) was used here except in Section 3.5, where different PCMs were compared. Also, except Section 4.1, $\frac{V_{PCM}}{V} = 0.9$ was used for all other cases. The parameters studied are listed below:

- To compare heat sink without PCMs to those with various filling of PCMs: $\frac{V_{PCM}}{V} = 0, 0.3, 0.6, 0.9$;
- To study the effect of temperature difference between the input boundary temperature and the melting point of PCMs: $\Delta T = T_w - T_m = 5, 10, 15, 20, 25, 30$ K;
- To investigate the effect of temperature difference between input boundary temperature and melting point with step ($\Delta T = T_w - T_m = \pm B$ with interval of 20 s) and sine ($\Delta T = B \sin(\omega t)$) curve for cyclic melting/freezing cases;
- To study the effect of aspect ratio: $\chi = 0.125, 0.25, 0.5, 1, 2$;
- To study the effect of different PCMs.

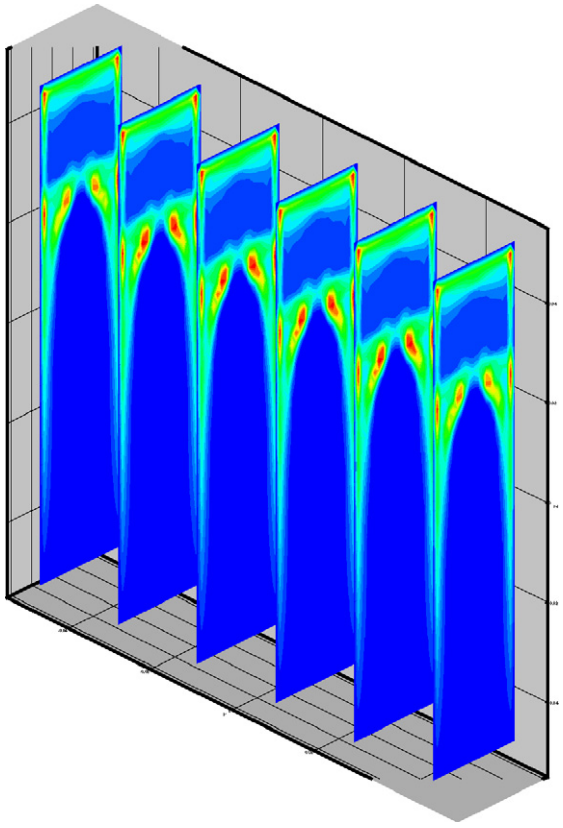

Fig. 4. Velocity contours at different slices at $t = 100$ min.

3.1. Heat sinks with/without PCMs

First, it is important to check the effect of inclusion of PCM on heat transfer characteristics of the heat sink. Four cases were selected here with initial PCM volume fraction with respect to the cavity volume as $\frac{V_{PCM}}{V} = 0, 0.3, 0.6$, and 0.9. It is noted that $\frac{V_{PCM}}{V} = 0$ represents the case of heat sink without PCMs. Fig. 5 shows evolution of normalized PCM melt fraction with time for the four cases. The legend shown in Fig. 5 is only adopted for this section. For the other sections in this paper, the melt volume fraction, ϕ, is normalized with reference to the PCM volume rather than the cavity volume. For a heat sink without PCMs, it is evident that the volume fraction is zero. When $\frac{V_{PCM}}{V}$ increases from 0.3 to 0.6, and to 0.9, the time for complete melting of PCMs (t_{max}) increases from 49.9 s to 70.0 s, and to 82.7 s, respectively. However, when the maximum volume fraction is doubled or tripled, the fully melting time is much less than two- or three-fold. The reason is that with the increased height of PCM inside the cavities of the heat sink, the effect of free convection is enhanced and results in faster melting.

Fig. 6 displays detailed melt volume fraction plots for different cases of heat sinks with PCMs at $t = 30$ s. It is noted that only one cell of the whole heat sink is demonstrated here considering the similar phenomena in each cavity inside the heat sink since the difference between different cavities is small. For all the three cases shown in the figure, complete melting of the PCM has not been reached yet. First, melting occurs over the hot surface, the side walls and the top empty cavity. Hence, the

melting of middle PCM part is slowest and causes the curved solid-liquid interface. Second, with increased volume of PCM, natural convection inside the liquid PCM is enhanced; this results in accelerated melting of the solid due to improved convection motion. The enhancement is also reflected in Fig. 5 that the melt rate is higher for larger PCM volume (V_{PCM}). It should be noted that in practical application, the volume occupied by the PCM will affect the fin's convective thermal performance due to the reduced effective length of the fin. The larger the PCM volume, the poorer the fin performance. Hence, there should be some optimized volume of the PCM to balance between the fin performance and the PCM performance. In the following sections, the maximum volume fraction of PCM is assumed to be $\frac{V_{\mathrm{PCM}}}{V} = 0.9$.

Fig. 7 demonstrates the evolution of temperature profile with time at a specific point in the domain (Point 2, as noted in Fig. 1) for different heat sinks with PCMs. For the case without PCMs ($\frac{V_{\mathrm{PCM}}}{V} = 0$), the specified local temperature sharply reaches the

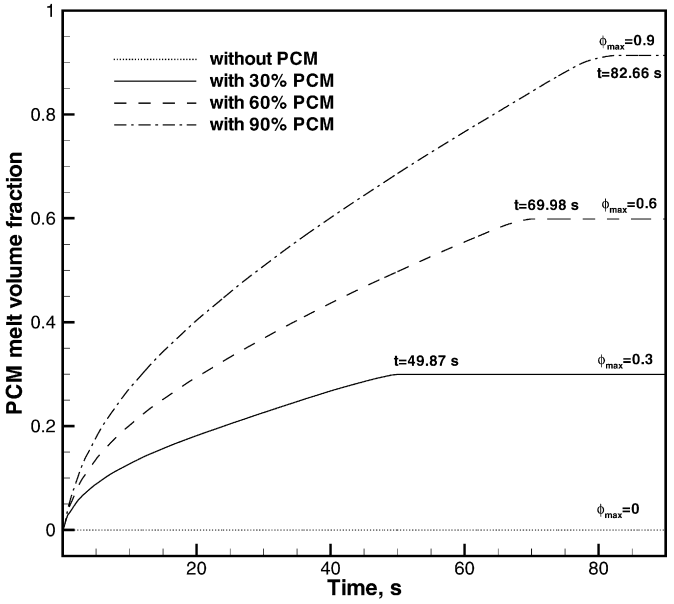

Fig. 5. Comparison between melting PCM melt volume fraction with time for heat sinks with and without PCMs. $\frac{V_{\mathrm{PCM}}}{V}$ is ratio between solid PCM volume and the whole cavity volume in the heat sink.

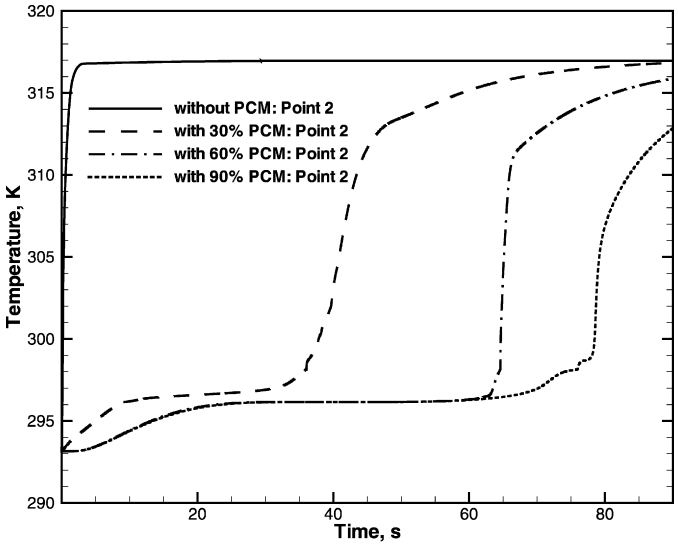

(a) Point 2

Fig. 7. Evolution of temperature with time for different heat sinks with/without PCMs at Point 2 (refer to Fig. 1, paraffin wax with $T_w - T_m = 20$ K).

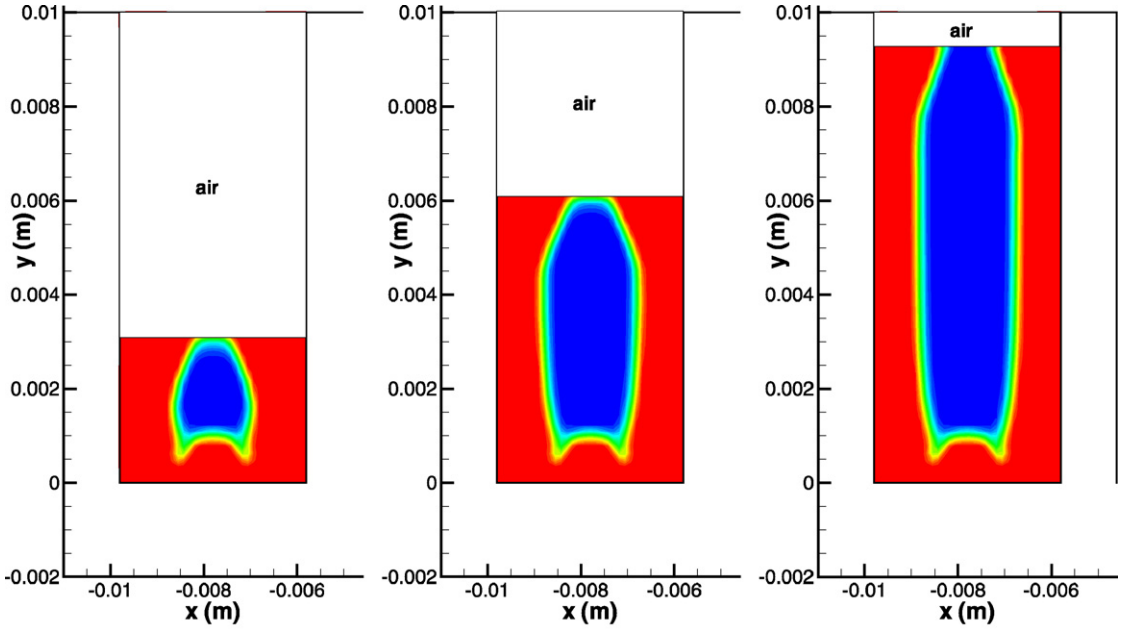

(a) $\frac{V_{\mathrm{PCM}}}{V} = 0.3$ (b) $\frac{V_{\mathrm{PCM}}}{V} = 0.6$ (c) $\frac{V_{\mathrm{PCM}}}{V} = 0.9$

Fig. 6. Liquid PCM volume fraction distribution for different heat sinks with PCMs at $t = 30$ s. The red color represents fluid PCM phase, while blue for solid PCM phase (paraffin wax with $T_w - T_m = 20$ K). (For interpretation of the references to color in this figure legend, the reader is referred to the web version of this article.)

boundary temperature. The delay is just caused by the conduction in the wall and the low convection in the air. As compared to empty cavity, the inclusion of PCMs delays the increase of the local temperature, as shown in Fig. 7. For each case with PCMs, the local temperature increases slowly from the initial value to the melting point of PCM first. The reduced slope is attributed to the heat capacity of the solid PCM inside, which is much higher than that of air for the case without PCMs. After reaching its melting point, the PCM starts melting. During the melting of PCM, due to the fixed melting point of PCM, the local temperature can be kept constant for a certain period, which is dependent on the PCM volume in the cavities. For a larger PCM volume, the constant temperature duration is longer. When the PCM is fully melted, only free convection within the liquid PCM and the top air prevail, so the local temperature will increase gradually from the melting point of PCMs to the boundary temperature, finally.

The numerical results show that the hybrid heat sink with specific PCMs has advantages as compared to the non-PCM heat sink. The inclusion of PCM stabilizes the local temperature at the desired value only if the PCM has not melted fully. Also, the included PCM can act as additional buffer system for extreme environments, e.g., the main cooling system is off or broken for a while. The PCMs can be utilized for such situations to allow the recovery of the main system rather than to shut down the electronic devices totally.

3.2. Effect of temperature difference ΔT

Fig. 8 presents the evolution of the melted volume fraction with time for various temperature differences ($\Delta T = T_w - T_m$) between the bottom input boundary temperature and the melting point of the PCM. The curves are displayed for $\Delta T = 5$, 10, 15, 20, 25, and 30 K. As expected, the larger the temperature difference, the higher is the melting speed, and the shorter is the time for complete melting. To compare the melting time for a specified melt volume fraction, cases $\phi = 0.3$ and $\phi = 0.6$ for $\frac{V_{\mathrm{PCM}}}{V} = 0.9$ are selected as examples, and shown in Table 3. For a fixed temperature difference, when the melt fraction is doubled from $\phi = 0.3$ to 0.6, the melting time is much higher than two-fold. Due to the enhanced natural convection during the melt for increased temperature difference (ΔT), the melting time at specified volume fraction (ϕ) decreases gradually. For example, for $\phi = 0.3$, when the temperate difference increases from 5 to 30 °C, the melting time decreases from 23.12 s to 4.70 s accordingly. Similar trends can be observed for $\phi = 0.6$.

Fig. 9 shows the calculated average heat transfer coefficient ($h' = q''/(T_w - T_{\mathrm{ref}})$, $T_{\mathrm{ref}} = T_{\mathrm{amb}}$ here) over the bottom surface of the heat sink as a function of time for various temperature differences. Similar to the results of melt volume fraction, the heat flux transferred to the PCM is maximum at the beginning and approaches the natural convection limit when the melting is complete. The larger the temperature difference, ΔT, the higher is the heat flux initially, and the steeper is the decrease in heat flux. It is noted that the total heat flux from the base could be the sum of the flux transferred into the PCM directly from the base and the flux transferred into the PCM through the surface

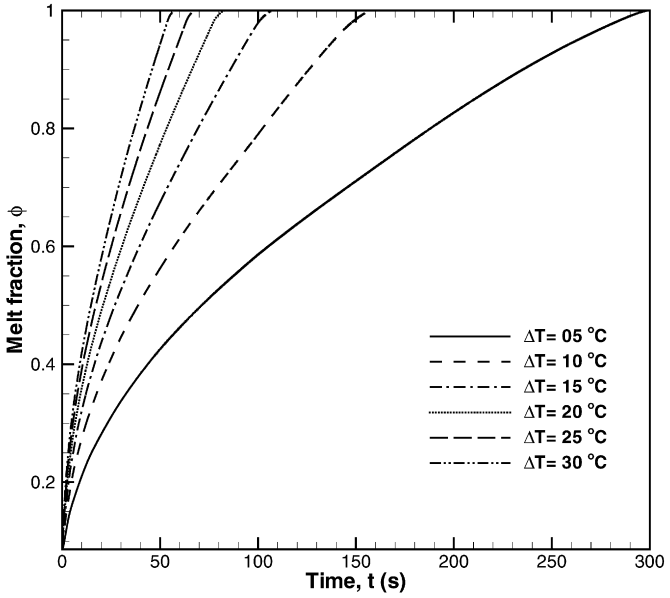

Fig. 8. Evolution of the melt fraction (ϕ) with time for various temperature differences.

Table 3
Melt fraction versus time

t (s)	ΔT (K)					
	5	10	15	20	25	30
$\phi = 0.3$	23.12	12.28	8.50	6.60	5.48	4.70
$\phi = 0.6$	105.25	57.28	39.49	30.54	25.11	21.38

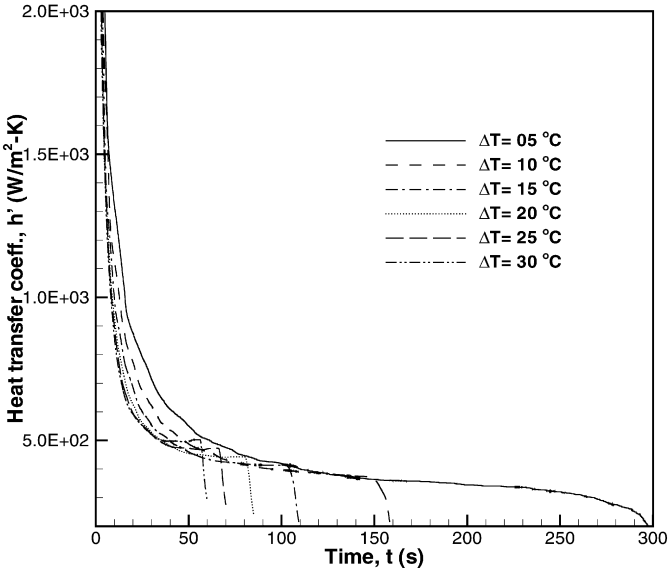

Fig. 9. Evolution of the average heat transfer coefficient ($\bar{h'}$) over the bottom surface ($y = -2$ mm) with time for various temperature differences.

of the fins. For a small system as discussed here, when the PCM layer between the fins is thicker, larger part of the total heat will be transferred directly from the base to the PCM.

In order to illustrate the difference in the melting process at different temperature differences, the predicted melt volume

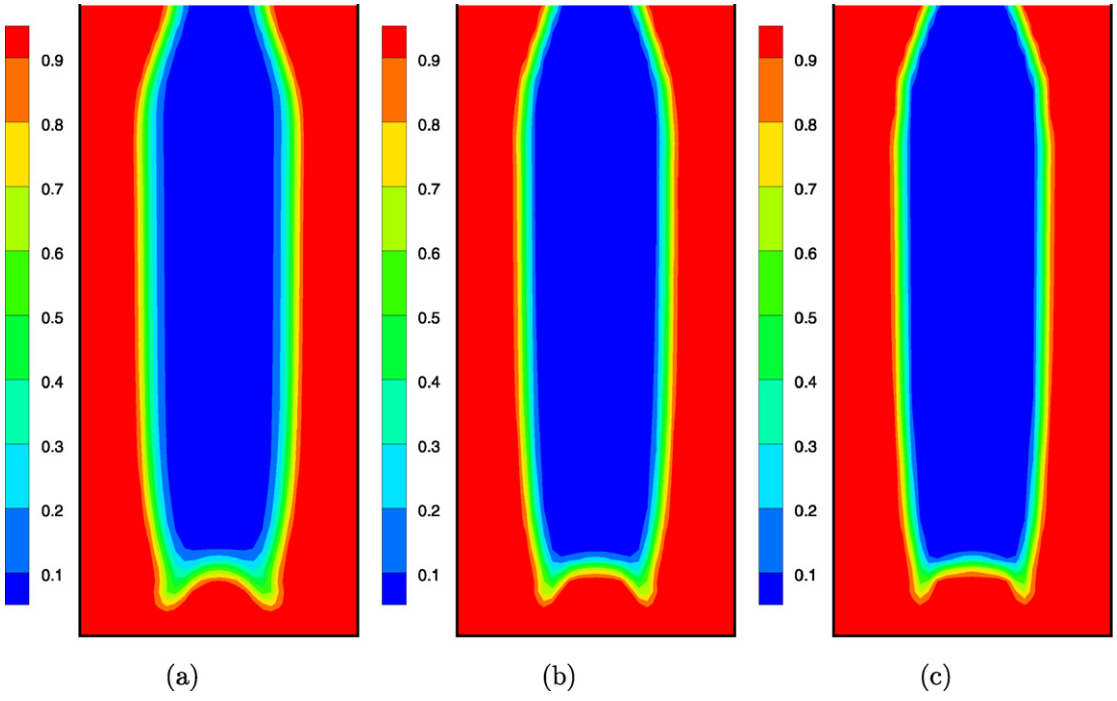

Fig. 10. Contours of the melt fraction of PCM at $\phi = 0.6$ for case: (a) $\Delta T = 10$ K; (b) $\Delta T = 20$ K; (c) $\Delta T = 30$ K.

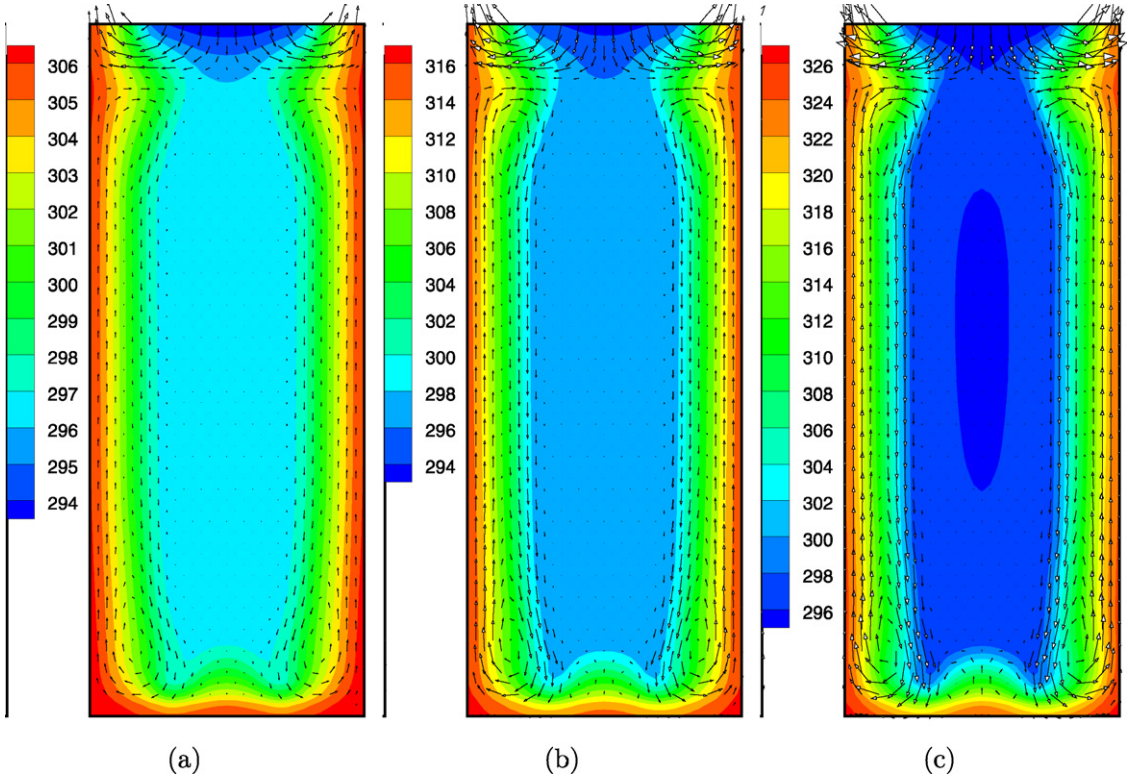

Fig. 11. Temperature distribution and velocity vector plots for liquid PCM at $\phi = 0.6$ for case: (a) $\Delta T = 10$ K; (b) $\Delta T = 20$ K; (c) $\Delta T = 30$ K.

fraction distributions are demonstrated in detail for $\Delta T = 10$, 20, and 30 K in Fig. 10 (a), (b), and (c), respectively. The phase distribution corresponds to melt fraction $\phi = 0.6$ as an instance. Note that the top air phase part is not included in the figure. It can be seen that for the fixed melt fraction, the phase distribution is nearly the same for the three cases. The melt front moves generally parallel to the vertical fins except near the top and bottom corners.

Fig. 11 shows both the temperature and velocity vector distributions for selected cases as discussed in Fig. 10. Results

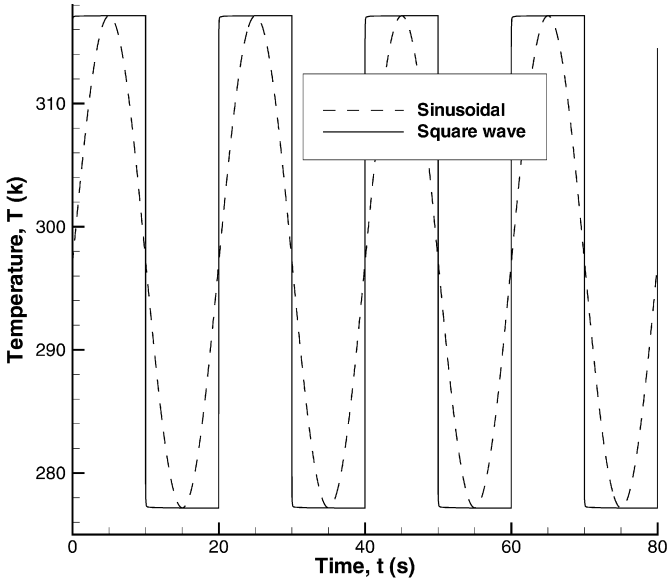

Fig. 12. Evolution of boundary temperature (T_w) with time for two boundary temperature profiles: sinusoidal curve and stepped curve.

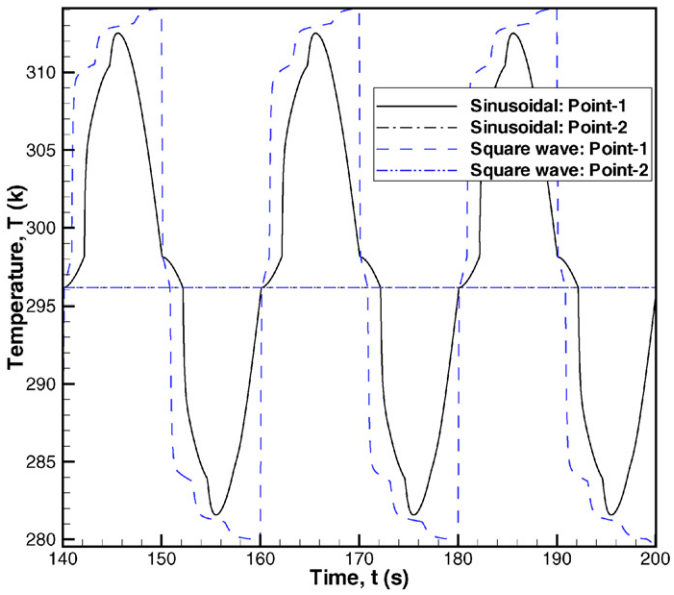

Fig. 13. Evolution of temperature at Points 1 and 2 (shown in Fig. 1) with time for two boundary temperature profiles: sinusoidal curve and stepped curve.

indicate that the increased temperature difference (ΔT) causes increased velocity, which is denoted by vector arrows with length for magnitude. Furthermore, the convective motion in the air phase is enhanced by the increased temperature difference. This is self-explanatory since the natural convection is related to temperature difference.

3.3. Effect of time-varying temperature difference

After discussion of constant time invariant temperature difference, it is interesting to study the effect of pulsed temperature difference during cyclic steady state of PCM's melting/freezing. Here two types of pulsed temperature differences are carried out, namely sinusoidal curve and stepped curve, which are schematically shown in Fig. 12 for selected cycles. The formulas are shown as follows (note that B and ω was arbitrarily chosen here):

$$\text{Sine pulsed } \Delta T: \quad \Delta T = T_w - T_m = B\sin(\omega t), \quad B = 20\ \text{K}, \omega = 2\pi/20 \tag{7}$$

$$\text{Step pulsed } \Delta T: \quad \Delta T = B, 2n < \frac{t}{20} \leqslant 2n+1; \quad \Delta T = -B, 2n+1 < \frac{t}{20} \leqslant 2(n+1) \tag{8}$$

Fig. 13 shows the local temperature variation with time at two monitored points (Points 1 and 2) in Fig. 1 for the two boundary temperature profiles. Considering that the growth of PCM melt develops from the walls to the center of the cavity, Point 2 does not melt during the cyclic melting period. Hence, the variation of temperature at Point 2 can be neglected, while temperature at Point 1 displays some interesting trends. For the case of stepped boundary temperature profile, the increase of local temperature is faster than the case of the sinusoidal boundary temperature profile. The plot of local temperature for both cases is more irregular than the boundary profiles. The difference between the two cases is that the crest of the stepped case is relatively sharper and the increasing rate is rather lower.

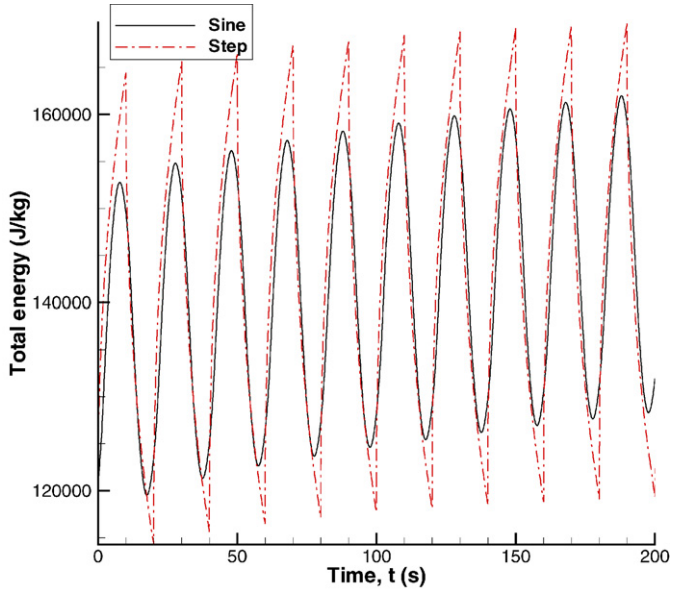

Fig. 14. Evolution of the total energy stored with time for two cases: sinusoidal curve and stepped curve.

The evolution of total energy storage with time for the sinusoidal and stepped cases is displayed in Fig. 14. First, for both cases, steady state can be reached in around 10 periods. As compared to the sinusoidal curve, the maximum stored energy for stepped curve case is much larger. It can be seen from Fig. 12 that the integration of temperature with time for stepped curve is relatively larger. Although only two typical regular curves were discussed here, some general results can be observed. For example, the internal local temperature depends on the input boundary temperature, but with delay in time.

3.4. Effect of aspect ratio

Since the space available for cooling in electronic device is limited, it is important to investigate the effect of physical aspect ratios of the PCM cartridge on the cooling performance of heat sinks. For simplification, three typical aspect ratios (or various widths, while the height and number of PCM cavities were held constant) were selected for the present study which are summarized in Table 4. Except for the listed scales, all other parameters are held the same as in previous sections as summarized in Table 1. Note that q'' was held constant rather than $\int q'' \, dx$ here. In all cases explored in this study, the model PCM has the properties of a commercially available paraffin wax.

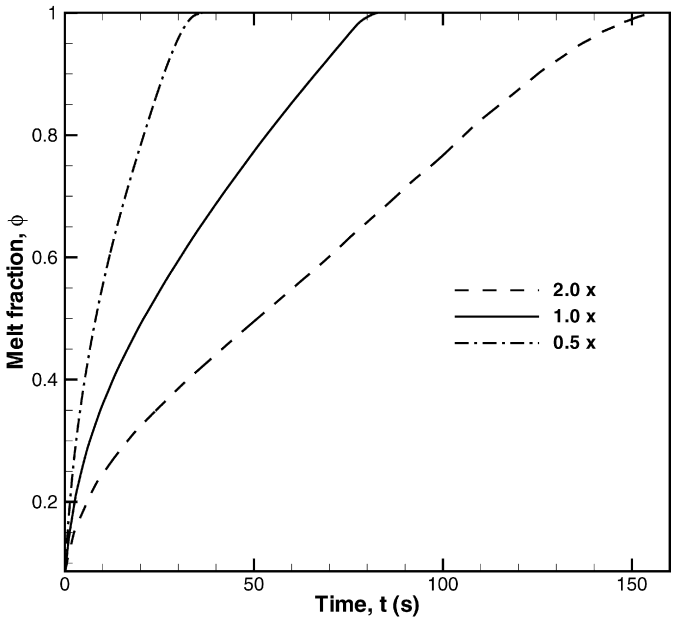

Fig. 15. Evolution of melt fraction (ϕ) with time for various aspect ratios.

Table 4 also shows time for typical melt fraction for the three aspect ratios $\alpha = 0.5$, 1, 2. Note that larger ratios represent wider PCM cartridges. It is found that, for the same melt fractions $\phi = 0.3$, 0.6, the melting time increases with increased aspect ratios. Furthermore, the increase in melting time is not linear with scales. For doubled aspect ratios (from 0.5 to 1, or from 1 to 2), the required time interval for same melt fraction is larger than twofold (from $t = 2.97$ to 6.60 s, or from $t = 6.60$ to 16.61). This means the heat transfer in the PCM is not only conduction-controlled, but also determined by convec-

Table 4
Geometry parameters and melt fraction versus time

Case	l_f (mm)	l_t (mm)	l_b (mm)	t (s) for $\phi = 0.3$	t (s) for $\phi = 0.6$
2×	10	2.4	8	16.61	69.70
1×	10	1.2	4	6.60	30.54
$\frac{1}{2}$×	10	0.6	2	2.97	11.72

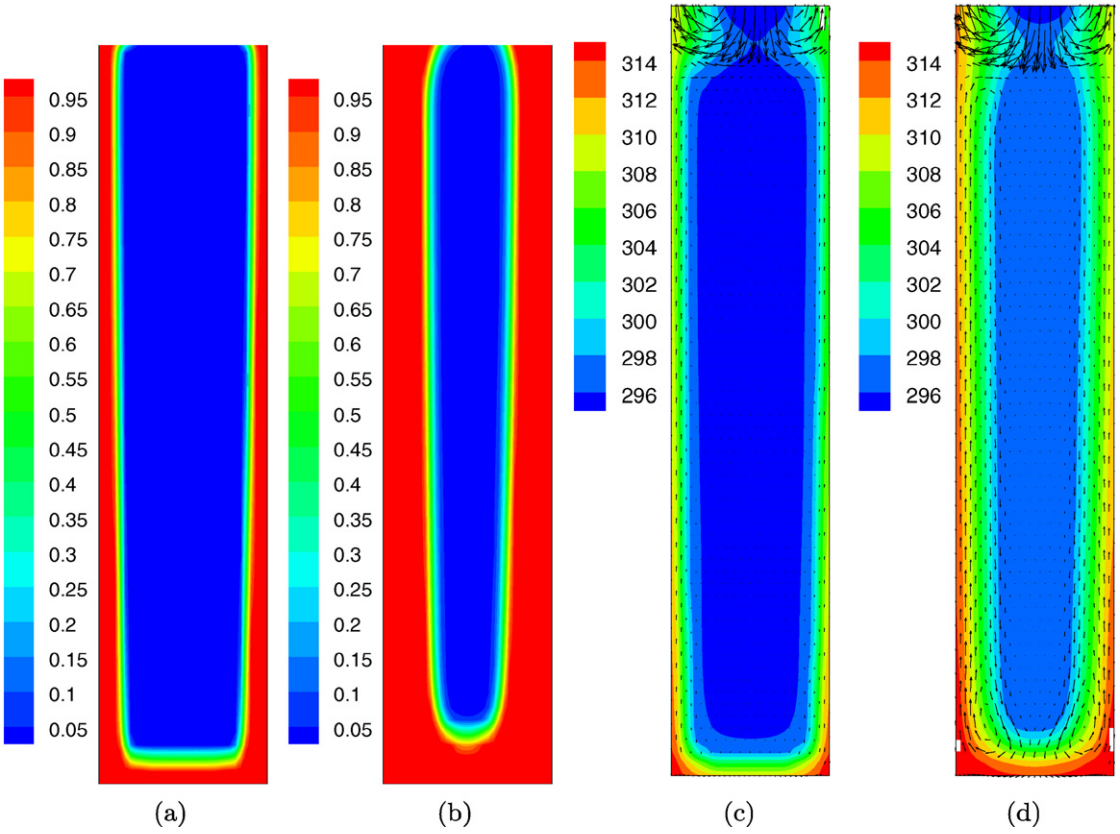

Fig. 16. Melt fraction distributions for $\alpha = 0.5$: (a) $\phi = 0.3$, (b) $\phi = 0.6$; temperature and velocity vector distribution for $\alpha = 0.5$: (c) $\phi = 0.3$, (d) $\phi = 0.6$.

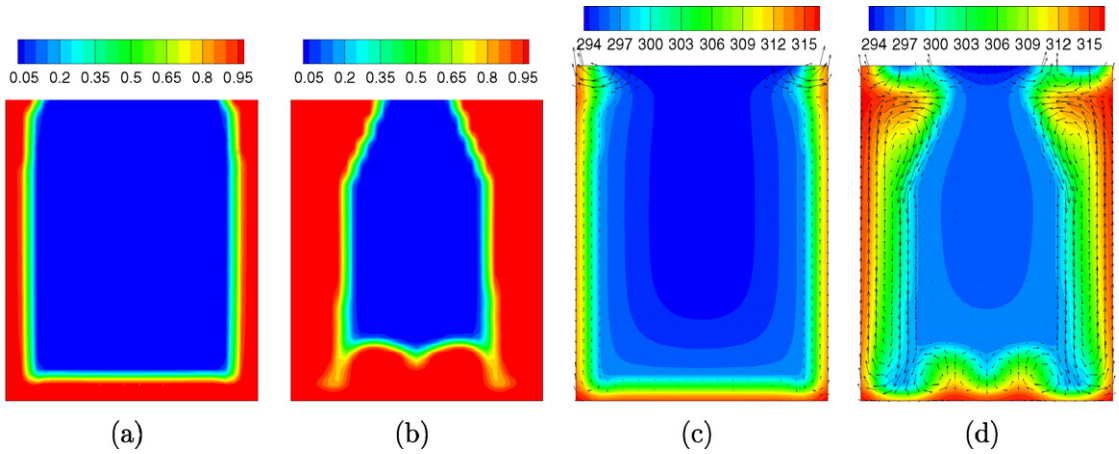

Fig. 17. Melt fraction distributions for $\alpha = 0.5$: (a) $\phi = 0.3$, (b) $\phi = 0.6$; temperature and velocity vector distribution for $\alpha = 0.5$: (c) $\phi = 0.3$, (d) $\phi = 0.6$.

Table 5
Properties of various PCM materials

	ρ (kg/m^3)	c_p (J/kg-K)	k (W/m-K)	T_m (°C)	ΔH (J/kg)
Eicosane	$\frac{785}{0.001(T-309.15)+1}$	2460	0.15	36	247 000
Heneicosane	$\frac{788}{0.001(T-313.55)+1}$	−(2500)	0.15	40.4	213 000
Suntech P116	$\frac{818}{0.001(T-320.15)+1}$	2730	0.24	47	266 000

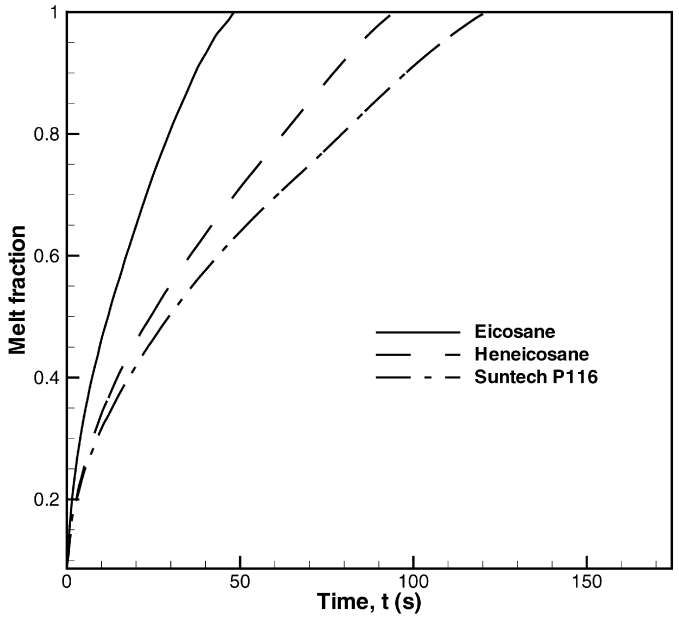

Fig. 18. Evolution of melt fraction (ϕ) with time for different PCMs.

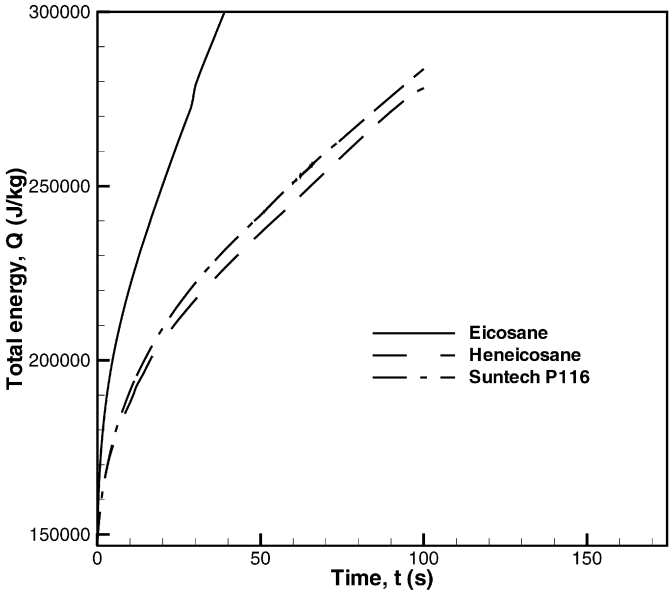

Fig. 19. Evolution of total energy (Q) with time for different PCM materials.

tion. Natural convection will be less effective at the wider scale, as explained in the later section.

The plots of the melt fraction (ϕ) with time for the three cases are shown in Fig. 15. For small aspect ratios or decreased width of the PCM layer, the melt fraction grows more rapidly with time. The melting rate decreases when the melt fraction reaches $\phi = 1$, which can be attributed to the interaction between the PCM phase with the adjacent low temperature air.

To illustrate the difference in the melting process for different dimensional scales, the melt fraction and velocity vector distributions for selected melt fraction ($\phi = 0.3$ and 0.6) are displayed in Figs. 16 and 17 for $\alpha = 0.5$ and $\alpha = 2$. For the case $\alpha = 1$, we refer to Figs. 10 and 11 for purpose of comparison. First, for melt fraction distribution, one can seen from Figs. 16 (a–b) and 17 (a–b) that at low melt fractions, for the wide PCM cases the melt front moves generally parallel to the vertical fin. As the width decreases, a wedge-like liquid phase is formed at the base. This means that for thick fins melting is nearly uniform along the fin surface, while for the thin cases melting takes place mostly close to the base. However, at a high melt fraction ($\phi = 0.6$), natural convection dominates in the liq-

uid phase. This involves complexity in wide cases such as $\alpha = 2$ considering that the original vortex at the bottom breaks into two, as shown in Fig. 17 (b) and (d). The splitting of the vortex affects the front curves significantly so that a strange front shape is formed, Fig. 17 (b). Second, for the velocity vector distributions, since the same vector unit is used, the increased physical scale decreases the global vector values somewhat, especially near the top air region.

3.5. Effect of PCM properties

The selection of appropriate PCM is important in the design of hybrid heat sinks. In this section, three commercial PCM materials (Eicosane, Heneicosane, and Suntech P116) were selected for comparison. Their thermal properties are shown in Table 5 [19,39,40]. Note that the initial temperature is $T_i = 308.15$ K, while the input boundary temperature is $T_w = 353.15$ K. Other parameters are kept as same.

Fig. 18 shows the evolution of melt fraction with time for the three PCMs. It can be seen that eicosane has the fastest melting, followed by heneicosane and Suntech P116. The main reason for this behavior is that the temperature difference between the boundary temperature and fusion point of eicosane is the largest. Although there are some differences in latent heat, it has insignificant effect on the results.

The related plot of total energy stored in the sink with time for the three PCMs are displayed in Fig. 19. It is interesting to find from these figures that eicosane has the highest energy storage, which is consistent with the melt fraction plot. But it is followed by Suntech P116 and then heneicosane, which is different from the melt fraction trends. Due to its higher specific heat, thermal conductivity and latent heat, the total energy content of Suntech P116 is greater than that of Heneicosane. This implies that for different PCMs, other than the melting point, ρ, c_p, k, and ΔH are also important factors.

Fig. 20 demonstrates the time-evolution of temperature at Point 3 for the three PCMs. Before the local temperature reaches the PCM's fusion point, the temperature increase results from heat conduction in the solid PCM, hence the melting rate is low. The local temperature remains constant when it

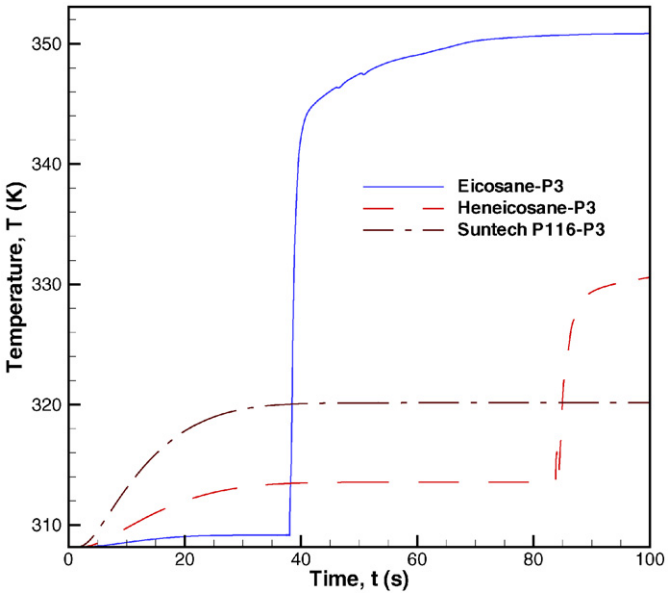

Fig. 20. Evolution of temperature at Point 3 (shown in Fig. 1) with time for different PCM materials.

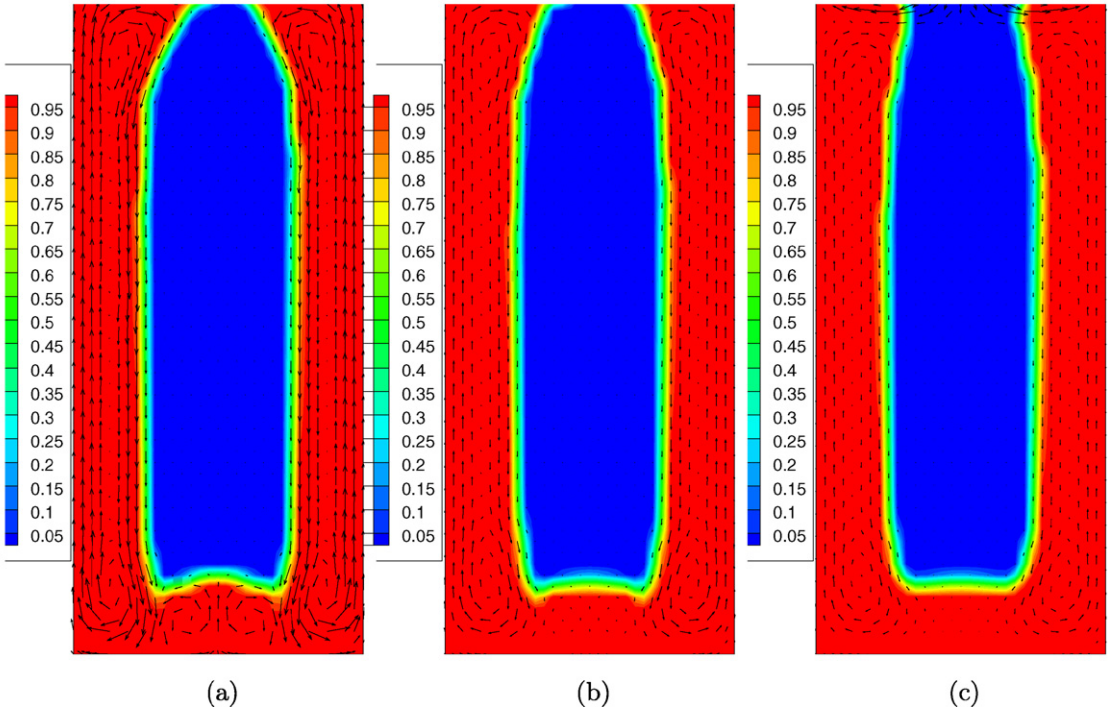

Fig. 21. Melt fraction distribution at $\phi = 0.6$ for different PCM materials: (a) Eicosane ($t = 17$ s); (b) Heneicosane ($t = 35.5$ s); (c) Suntech P116 ($t = 43.6$ s).

reaches the fusion point until the complete melting point. After complete melting, the local temperature increases sharply. Actually the constant temperature region is of interest for electronic cooling applications. Hence, the longer steady temperature the better.

The melt fraction and velocity vector distributions are shown in Fig. 21 for $\phi = 0.6$. We can see that the melt fraction distribution is nearly same for the three PCMs. However, the vector fields are different. Eicosane has stronger velocity fields than Heneicosane and Suntech P116. One possible reason is that the lowest melting point results in quickest melting and then stronger natural convection in liquid PCM. Suitable selection of PCM is necessary during the designing of hybrid heat sink. Not only the melting point, but also other thermal properties will affect the thermal performance of the whole cooling system.

4. Conclusion

A two-phase and conjugated computational model with 2D assumption was employed to study the hybrid PCM-based heat sinks. First, the numerical method was validated using experimental data from literature. Results show good agreement and reasonability of the 2D assumption. Then, some important parameters of the PCM-based heat sink were investigated. Results indicate that inclusion of PCM in the base heat sink will increase the thermal performance of the hybrid system under free convection conditions. Furthermore, constant and pulsed temperature difference between the input boundary temperature and melting point of the PCMs, aspect ratio, and various PCM properties are critical factors to affect the performance. Hence, appropriate selection of PCMs is essential for successful design of the cooling system.

References

[1] J. Bass, D. Allen, S. Ghamaty, N. Elsner, New technology for thermoelectric cooling, in: 20th IEEE SEMI-THERM Symposium, 2004, pp. 18–20.

[2] A.R. Tilley, H.D. Associates, The Measure of Man and Women, Human Factors in Design, revised edition, Whitney Library of Design, Watson–Guptill Publications, 2001.

[3] Z.X. Gong, A.S. Mujumdar, Cyclic heat transfer in a novel storage unit of multiple phase change materials, Applied Thermal Engineering 16 (10) (1996) 807–815.

[4] Z.X. Gong, A.S. Mujumdar, Enhancement of energy charge–discharge rates in composite slabs of different phase change materials, International Journal of Heat and Mass Transfer 39 (4) (1996) 725–733.

[5] Z.X. Gong, A.S. Mujumdar, Thermodynamic optimization of the thermal process in energy storage using multiple phase change materials, Applied Thermal Engineering 17 (11) (1997) 1067–1083.

[6] Z.X. Gong, A.S. Mujumdar, A finite element model for convection-dominated melting and solidification problems, International Journal of Numerical Methods for Heat and Fluid Flow 8 (4) (1998) 393–408.

[7] Z.X. Gong, S. Devahastin, A.S. Mujumdar, Enhanced heat transfer in free convection-dominated melting in a rectangular cavity with an isothermal vertical wall, Applied Thermal Engineering 19 (1999) 1237–1251.

[8] Z.X. Gong, A.S. Mujumdar, A new solar receiver thermal store for space-based activities using multiple composite phase change materials, ASME Journal of Solar Energy Engineering 117 (1995) 215–220.

[9] Z.X. Gong, A.S. Mujumdar, Exergetic analysis of thermal storage using multiple phase change materials, ASME Journal of Energy Resources Technology 118 (1996) 242–248.

[10] G. Casano, S. Piva, Experimental and numerical investigation of the steady periodic solid–liquid phase-change heat transfer, International Journal of Heat and Mass Transfer 45 (20) (2002) 4181–4190.

[11] L.M. Jiji, S. Gaye, Analysis of solidification and melting of PCM with energy generation, Applied Thermal Engineering 26 (2006) 568–575.

[12] R. Velraj, R.V. Seeniraj, B. Hafner, C. Faber, K. Schwarzer, Heat transfer enhancement in a latent heat storage system, Solar Energy 65 (3) (1999) 171–180.

[13] B. Zalba, J.M. Marin, L.F. Cabeza, H. Mehlin, Free-cooling of building with phase change materials, International Journal of Refrigeration 27 (2004) 839–849.

[14] D. Pal, Y.K. Joshi, Melting in a side heated tall enclosure by a uniformly dissipating heat source, International Journal of Heat and Mass Transfer 44 (2001) 375–387.

[15] V. Kulish, J. Lage, Diffusion within a porous medium with randomly distributed heat sinks, International Journal of Heat and Mass Transfer 43 (2000) 3481–3496.

[16] J. Lage, A. Weinert, D. Price, R. Weber, Numerical study of a low permeability microporous heat sink for cooling phase-array radar systems, International Journal of Heat and Mass Transfer 39 (1996) 3633–3647.

[17] S. Krishnan, S. Garimella, Analysis of a phase change energy storage system for pulsed power dissipation, in: Proc. IEEE Trans. Compon. Packag. Technol., vol. 27, 2004, pp. 191–199.

[18] J. O'Conner, R. Weber, Thermal management of electronic packages using solid-to-liquid phase change techniques, International Journal of Microcircuits and Electronic Packaging 20 (1997) 593–601.

[19] J. Leland, G. Recktenwald, Optimization of phase change heat sink for extreme environments, in: Proceedings of the Nineteenth Annual IEEE Semiconductor Thermal Measurement and Management Symposium, Institute of Electrical and Electronics Engineers, Inc., San Jose, CA, USA, 2003.

[20] N. Zheng, R. Wirtz, Methodology for designing a hybrid thermal energy storage heat sink, in: Proceedings of the 2001 ASME International Mechanical Engineering Congress and Exposition, ASME, 2001, 2-16-2-10.

[21] N. Zheng, R. Wirtz, Figures of merit for hybrid thermal energy storage units, in: Proceedings of the 2001 ASME National Heat Transfer Conference, ASME, 2001, NHTC2001-20027.

[22] N. Zheng, R. Wirtz, A hybrid thermal energy storage device, part 1: design methodology, Journal of Electronic Packaging 126 (2004) 1–7.

[23] P. Lamberg, K. Siren, Approximate analytical model for solidification in a finite PCM storage with internal fins, Applied Mathematical Modelling 27 (2003) 491–513.

[24] F. Tan, C. Tso, Cooling of mobile electronic devices using phase change materials, Applied Thermal Engineering 24 (2004) 159–169.

[25] S. Krishnan, S. Garimella, S. Kang, A novel hybrid heat sink using phase change materials for transient thermal management of electronics, in: Proceedings of 2004 Inter Society Conference on Thermal Phenomena (ITHER M04), 2004, pp. 310–318.

[26] R. Akhilesh, A. Narasimhan, C. Balaji, Method to improve geometry for heat transfer enhancement in PCM composite heat sinks, International Journal of Heat and Mass Transfer 48 (13) (2005) 2759–2770.

[27] V. Shatikian, G. Ziskind, R. Letan, Numerical investigation of a PCM-based heat sink with internal fins, International Journal of Heat and Mass Transfer 48 (17) (2005) 3689–3706.

[28] M.J. Huang, P.C. Eames, B. Norton, Comparison of a small-scale 3D PCM thermal control model with a validated 2D PCM thermal control model, Solar Energy Materials and Solar Cells 90 (13) (2006) 1961–1972.

[29] V. Voller, M. Cross, N. Markatos, An enthalpy method for convection/diffusion phase change, International Journal of Numerical Methods for Engineering 24 (1987) 271–284.

[30] A. Brent, V. Voller, K. Reid, Enthalpy-porosity technique for modeling convection–diffusion phase change: application to the melting of a pure metal, Numerical Heat Transfer, Part A 13 (1988) 297–318.

[31] C. Hirt, B. Nichols, Volume of fluid (VOF) method for the dynamics of free boundaries, Journal of Computational Physics 39 (1981) 201.

[32] W. Humphries, E. Griggs, A design handbook for phase change thermal control and energy storage devices, Tech. Rep., 1074NASA Scientific and Technical Information Office, 1977.

[33] R. Reid, J. Prausnitz, B. Poling, The Properties of Gases and Liquids, McGraw–Hill, New York, 1987.
[34] http://www.fluent.com.
[35] M. Pinelli, G. Casano, S. Piva, Solid–liquid phase-change heat transfer in a vertical cylinder heated from above, International Journal of Heat and Technology 18 (1999) 61–67.
[36] M. Pinelli, S. Piva, Solid/liquid phase change in presence of natural convection: A thermal energy storage case study, Journal of Energy Resources Technology 125 (2003) 190–197.
[37] D. Caudwell, J. Trusler, V. Vesovic, W. Wakeham, The viscosity and density of *n*-dodecane and *n*-octadecane at pressures up to 200 MPa and temperatures up to 473 K, International Journal of Thermophysics 25 (5) (2004) 1339–1352.
[38] M. Zukowski, Mathematical modeling and numerical simulation of a short-term thermal energy storage system using phase change material for heating applications, Energy Conversion and Management 48 (1) (2007) 155–165.
[39] S. Himran, A. Suwono, G. Mansoori, Characterization of alkanes and paraffin waxes for application as phase change energy storage medium, Energy Sources 16 (1994) 117–128.
[40] F. Incropera, D.D. Witt, Fundamentals of Heat and Mass Transfer, Wiley, New York, 1998.
[41] B. Zivkovic, I. Fujii, An analysis of isothermal phase change of phase change material within rectangular and cylindrical containers, Solar Energy 70 (1) (2001) 51–61.